Supplementary Material: Subglacial Canal Initiation Driven by Till Erosion

Indraneel Kasmalkar, Elisa Mantelli, Jenny Suckale

1 Linearization of the Exner Equation

We introduce the perturbation $\exp(ik_1x + ik_2y + \omega t)$ into the non-dimenstional Exner equation (3.3) from the manuscript. Omitting the star notation for non-dimensional variables,

$$\omega r' = -ik_1 q_x' - ik_2 q_y', \quad \mathbf{q}' = F(\mathrm{S}|\overline{\boldsymbol{\tau}}|)\hat{\boldsymbol{\tau}}' + \mathrm{S}|\boldsymbol{\tau}|'\mathrm{d}F(\mathrm{S}|\overline{\boldsymbol{\tau}}|)\overline{\hat{\boldsymbol{\tau}}}. \tag{S.1}$$

The non-dimensional bed stress $\boldsymbol{\tau} = (\tau_x, \tau_y)$ and unit bed stress vectors are given by (2.8),

$$\tau_i = \mathbf{t}_i^T \left(\nabla \mathbf{u} + \nabla \mathbf{u}^T\right)\mathbf{n}, \quad \hat{\boldsymbol{\tau}} = \frac{\boldsymbol{\tau}}{|\boldsymbol{\tau}|}, \quad \text{at} \quad z = r. \tag{S.2}$$

The vectors $\mathbf{t}_x, \mathbf{t}_y$ are the unit tangent vectors to the bed in the x- and y- directions respectively, and $\mathbf{n}$ is the normal surface vector for the bed $z = r(x, y, t)$,

$$\mathbf{t}_x = \frac{\left(1, 0, \frac{\partial r}{\partial x}\right)}{\sqrt{1 + \left(\frac{\partial r}{\partial x}\right)^2}}, \quad \mathbf{t}_y = \frac{\left(1, 0, \frac{\partial r}{\partial y}\right)}{\sqrt{1 + \left(\frac{\partial r}{\partial y}\right)^2}}, \quad \mathbf{n} = \frac{\left(-\frac{\partial r}{\partial x}, -\frac{\partial r}{\partial y}, 1\right)}{\sqrt{1 + \left(\frac{\partial r}{\partial x}\right)^2 + \left(\frac{\partial r}{\partial y}\right)^2}}. \tag{S.3}$$

After introducing the perturbations, these vectors take the form,

$$\mathbf{t}_x = (1,0,0) + \varepsilon i k_1 r'(0,0,1), \quad \mathbf{t}_y = (1,0,0) + \varepsilon i k_2 r'(0,0,1), \quad \mathbf{n} = (0,0,1) + \varepsilon(ik_1 r', ik_2 r', 0). \tag{S.4}$$

We evaluate the non-dimensional stress terms and their perturbations,

$$\overline{\boldsymbol{\tau}} = (1,0), \quad \boldsymbol{\tau}' = (\mathrm{D}u' + ik_1 w', \mathrm{D}v' + ik_2 w'), \quad \overline{\hat{\boldsymbol{\tau}}} = (1,0), \quad \hat{\boldsymbol{\tau}}' = (0, \mathrm{D}v' + ik_2 w'). \tag{S.5}$$

Care needs to be taken for the computation for $\hat{\boldsymbol{\tau}}' = \left(\frac{\boldsymbol{\tau}}{|\boldsymbol{\tau}|}\right)'$. The perturbation of $|\boldsymbol{\tau}|$ is given by $|\boldsymbol{\tau}|' = 1 + \varepsilon \text{ Real}\left(\mathrm{D}u' + ik_1 w'\right)$. Thus,

$$\mathbf{q}' = \left([\mathrm{D}u' + ik_1 w']\,\mathrm{S}\mathrm{d}F(\mathrm{S}) \;\;,\;\; F(\mathrm{S})\,[\mathrm{D}v' + ik_2 w']\right), \tag{S.6}$$

which yields the linearized Exner equation (5.10),

$$\omega r' = -ik_1 \mathrm{S}\kappa \mathrm{d}F\,[\mathrm{D}u' + ik_1 w'] - ik_2 \kappa F\,[\mathrm{D}v' + ik_2 w']. \tag{S.7}$$

2 Numerics

For reference, we write the main system of equations (5.20 - 5.23) from the manuscript,

$$\gamma\omega\left[\mathrm{D}^2 - k^2\right]\psi = -ik_1\left[\overline{u}\mathrm{D}^2\psi - \psi\mathrm{D}^2\overline{u} - k^2\overline{u}\psi\right] + \frac{1}{\mathrm{Re}}\left[\mathrm{D}^2 - k^2\right]^2\psi, \tag{S.7}$$

$$\mathrm{D}\psi = 0, \quad \psi = 0, \quad \text{at } z = 2, \tag{S.8}$$

$$\mathrm{D}\psi = -\sin(\theta)\mathrm{L}\mathrm{D}\overline{u}r', \quad \psi = 0, \quad \text{at } z = 0, \tag{S.9}$$

$$\omega r' = -ik\kappa F\mathrm{D}^2\psi \quad \text{at} \quad z = 0, \tag{S.10}$$

where $\psi(z)$ is the streamfunction, z corresponds to the coordinate along the film depth, Re is the Reynolds number, $\overline{u}(z)$ is the steady state velocity along the x-direction, r' is the bed-form perturbation amplitude, k is the perturbation wavenumber, F is the steady state non-dimensional bed-load flux value, θ is the Squire angle, $k_1 = k\sin\theta$ and κ is a non-dimensional variable that connects the model scaling to that of the standard bedload transport scaling. We present the details of spectral Galerkin solver for the equations (S.7 - S.10). For the purpose of the solver, we perform the translation $\zeta = z - 1$. We define the modified Sobolev space,

$$H^2_{\pm 1}[-1,1] = \left\{ \varphi \in L^2[-1,1] : \quad \varphi(\pm 1) = 0, \frac{d\varphi}{d\zeta}(\pm 1) = 0, \quad \frac{d^j\varphi}{d\zeta^j} \in L^2[-1,1], \quad 0 \le j \le 2 \right\}, \tag{S.12}$$

where $L^2[-1,1]$ is the space of all square-integrable functions on $-1 \le \zeta \le 1$.

We write (S.7) in weak form by integrating against $\varphi \in H^2_1[-1,1]$,

$$\omega M(\psi,\varphi) = A(\psi,\varphi), \tag{S.13}$$

where $M(\psi,\phi)$ and $A(\psi,\phi)$ are the mass and the stiffness bilinear forms, respectively,

$$M = \gamma\left[I_{20} - k^2 I_{00}\right], \quad A = ik_1\left[U_{200} - U_{020} + k^2 U_{000}\right] + \frac{1}{\mathrm{Re}}\left[I_{22} - 2k^2 I_{20} + k^4 I_{00}\right], \tag{S.14}$$

$$\text{and,} \quad I_{j_1 j_2}(\psi,\varphi) \int_{-1}^{1} \frac{d^{j_1}\psi}{d\zeta^{j_1}} \frac{d^{j_2}\varphi}{d\zeta^{j_2}} d\zeta, \quad U_{j_1 j_2 j_3}(\psi,\varphi) = \int_{-1}^{1} \frac{d^{j_1}\overline{u}}{d\zeta^{j_1}} \frac{d^{j_2}\psi}{d\zeta^{j_2}} \frac{d^{j_3}\varphi}{d\zeta^{j_3}} d\zeta. \tag{S.15}$$

In (S.14) we use integration by parts, combined with boundary terms equaling zero due to (S.12).

We approximate the solution space for ψ by the finite dimensional subspace,

$$V_N = \mathrm{Span}\{\psi_j : -1 \le j \le N\}, \tag{S.16}$$

where, for $1 \le j \le N$, we define ψ_j as the double-integrated Legendre polynomial L_{j+1} such that $\psi_j(\pm 1) = \frac{d\psi_j}{d\zeta}(\pm 1) = 0$, namely,

$$\psi_j = \sqrt{j + \frac{3}{2}}\left(\frac{L_{j+3} - L_{j+1}}{(2j+3)(2j+5)} - \frac{L_{j+1} - L_{j-1}}{(2j+1)(2j+3)}\right), \tag{S.17}$$

and ψ_0, ψ_1 correspond to two low-degree polynomials, linearly independent from the other ψ_j, to incorporate the two boundary conditions (S.9) at the till-water interface,

$$\psi_0(z) = (\zeta - 1)^2, \quad \psi_{-1}(z) = (\zeta - 1)^2(\zeta + 2). \tag{S.18}$$

We write the solution as $\psi = \sum_{j=-1}^{N} a_j \psi_j$. Note that the ice-water boundary conditions (S.8) would be automatically satisfied by any such ψ. We incorporate the boundary conditions (S.9) and the Exner equation (S.10) in strong form.

We approximate the test function space $H^2_{\pm 1}[-1,1]$ by the finite dimensional subspace W_N, which consists of just the standard basis functions without the low-degree polynomials.

$$W_N = \mathrm{Span}\{\psi_j : 1 \le j \le N\}. \tag{S.19}$$

We reformulate the bilinear forms A, I, U and M in (S.13) as $(N+3) \times (N+3)$ matrices. The $N+3$ columns stand the unknowns represented by $\mathbf{x} = (a_{-1}, a_0, a_1, ..., a_N, r')$. The $N+3$ rows stand for integration against the N test functions of W_N, plus three additional rows that describe the two boundary conditions (S.9) and the Exner equation (S.10). With we obtain a finite dimensional eigenvalue problem, $A\mathbf{x} = \omega M\mathbf{x}$, which we solve using the Matlab *eig* routine.

3 Asymptotic Analysis

3.1 Short Wavelength Diffusion

The analytical solution of the reduced model (6.7 - 6.10) for the short wavelength diffusion-only regime is given by,

$$\psi^{(0)} = -2z^{(0)}\exp(-z^{(0)}), \quad \omega^{(0)} = -4i, \tag{S.20}$$

We compare the theoretical value of ω, given above, and the rescaled numerical results, $\omega_{\mathrm{num}} = \frac{\omega}{F \mathrm{L} k^2 \sin\theta}$ in Figure S1. The figure shows good agreement between the numerical and theoretical solutions.

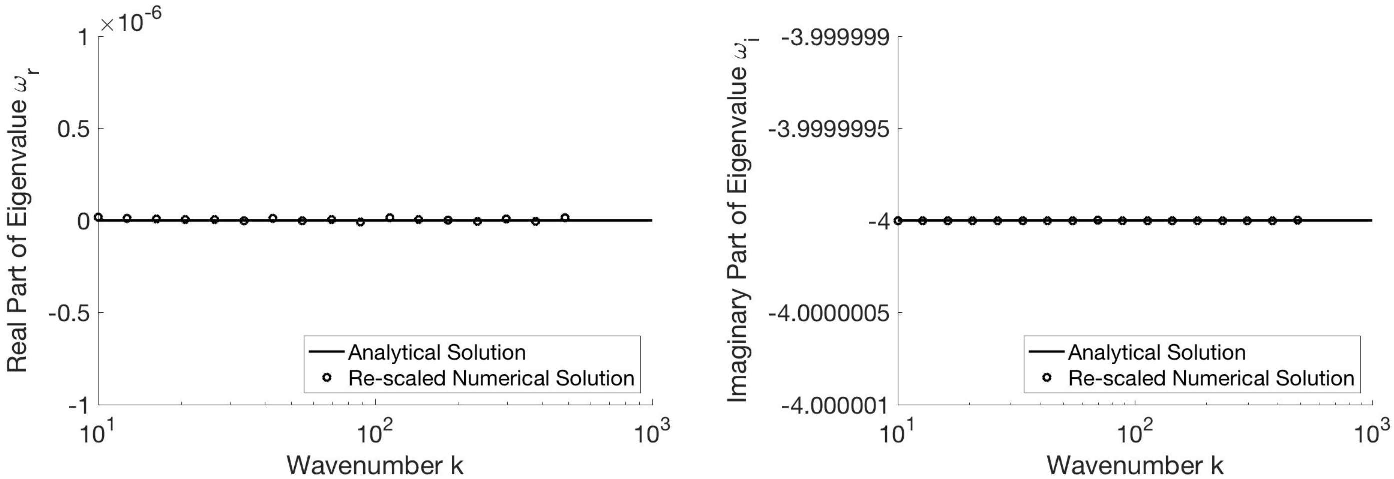

(a) Comparison for the real part, ω_r.

(b) Comparison for the imaginary part, ω_i.

Figure S1: Analytical and re-scaled numerical solutions for the short wavelength diffusion regime.

3.2 Long Wavelength Diffusion

The analytical solution of the reduced model (6.16 - 6.19) for the long wavelength diffusion-only regime is given by,

$$\psi = -2z + 2z^2 - 0.5z^3, \quad \omega = -4i, \tag{S.21}$$

We compare the theoretical value of ω, given above, and the rescaled numerical results, $\omega_{\text{num}} = \frac{\omega}{F\text{L}k\sin\theta}$. Figure S2 suggests that the numerical result converges to the theoretical value as $k \to 0$.

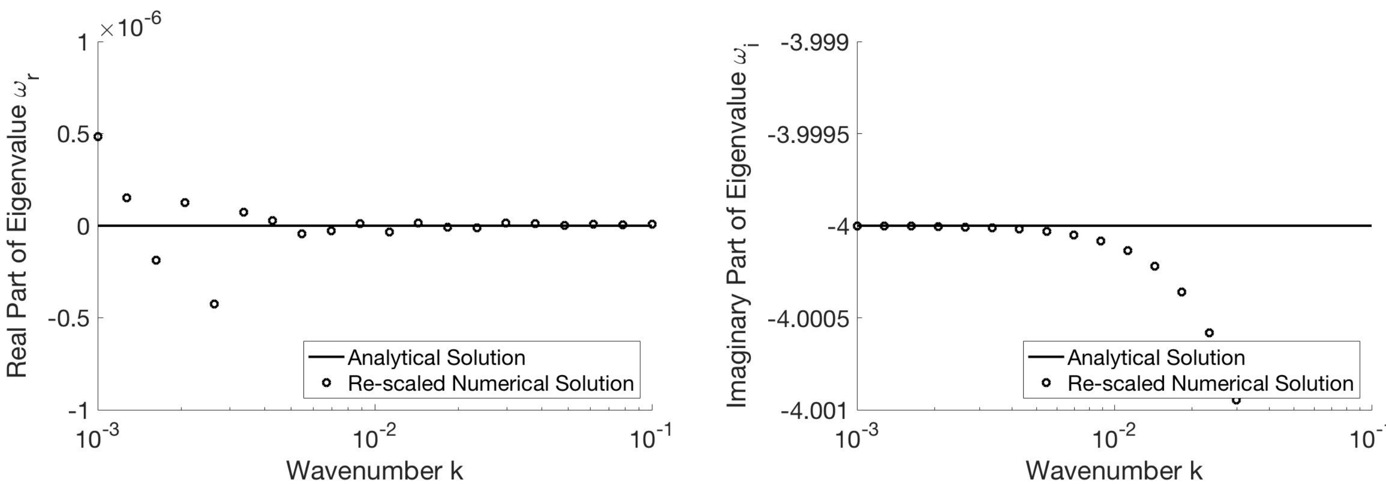

(a) Comparison for the real part, ω_r.

(b) Comparison for the imaginary part, ω_i.

Figure S2: Analytical and re-scaled numerical solutions for the long wavelength diffusion regime. (a) exhibits ill-conditioning as $k \to 0$.

3.3 Short Wavelength Advection

The analytical solution of the reduced model (6.21, 6.8 - 6.10) for the short wavelength advection-diffusion regime is given by,

$$\psi = \frac{2\int_0^z \int_v^\infty e^{2v-s-z}\mathrm{Ai}(c^{-1}s + c^2)dsdv}{\int_0^\infty e^{-s}\mathrm{Ai}(c^{-1}s + c^2)ds}, \quad \omega = \frac{-2i\mathrm{Ai}(c^2)}{\int_0^\infty e^{-s}\mathrm{Ai}\left(c^{-1}s + c^2\right)ds}, \tag{S.22}$$

where $c = \frac{1}{\sqrt[3]{2ia_2}}$ with $\arg(c) = -\frac{\pi}{6}$, and $\mathrm{Ai}(z)$ is one of the two standard linearly independent solutions of the system $\mathrm{D}^2 f = zf$. The integrals in (S.22) converge due to the exponential decay rate of $\mathrm{Ai}(z)$ for $-\frac{\pi}{3} < z < \frac{\pi}{3}$.

We compare the theoretical value of ω, given above, and the rescaled numerical results, $\omega_{\text{num}} = \frac{\omega}{F\mathrm{L}k^2 \sin\theta}$ in Figure S3.

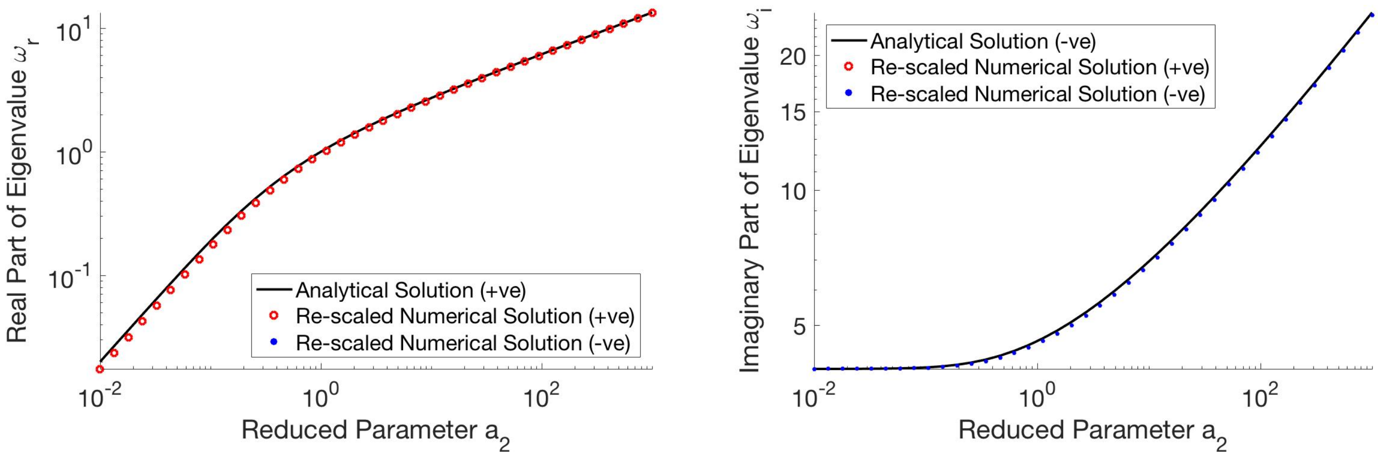

(a) Comparison for the real part, ω_r.

(b) Comparison for the imaginary part, ω_i.

Figure S3: Analytical and re-scaled numerical solutions for the short wavelength advection regime.

3.4 Long Wavelength Advection

We reduce the re-scaled OS equation (6.13) for long wavelengths ,

$$b_1\omega(D^{*2} - k^2)\psi^* = -ib_2\left[\left(2z^* - z^{*2}\right)(D^{*2} - k^2) + 2\right]\psi^* + (D^{*2} - 1)^2\psi^*, \tag{S.23}$$

by $b_1 \to 0$ to suppress acceleration, and an asymptotic expansion around $k = 0$ for the long wavelength regime,

$$ib_2\left[z^{(0)}\left(2 - z^{(0)}\right)\mathrm{D}^2 + 2\right]\psi^{(0)} = \mathrm{D}^4\psi^{(0)}, \quad b_2 = Rek\sin\theta. \tag{S.24}$$

We find a semi-analytic solution for (S.24), and the associated boundary conditions for the long wavelength regime (6.17 - 6.19) on $0 \le z \le 2$ via a Taylor expansion at $z = 0$. We solve the reduced model for the coefficients of $1, z, z^2, ..., z^{n-1}$, $n = 12$ using the Matlab sybolic toolbox. We compute $\mathrm{D}^2\psi^{(0)}(0)$ to first order,

$$\mathrm{D}^2\psi^{(0)}(0) = \frac{1436400ib_2^2 + 18711000b_2 - 98232750i}{-14336b_2^5 + 280704ib_2^4 + 2106720b_2^3 + 476280ib_2^2 + 7484400b_2 - 49116375i} + 2. \tag{S.25}$$

We assume $b_2 \ll 1$, which is justified for $\theta \ll 1$. We compute $\omega^{(0)}$ by approximating $\mathrm{D}^2\psi^{(0)}(0)$ with a first-order Taylor expansion at $b_2 = 0$,

$$\omega^{(0)} = \mathrm{D}^2\psi^{(0)}(0) \approx 4 + 0.762ib_2. \tag{S.26}$$

We compare the theoretical value of ω, given above, and the rescaled numerical results, $\omega_{\text{num}} = \frac{\omega}{F\mathrm{L}k\sin\theta}$. Figure S4 highlights that the numerical result converges to the theoretical value as $k \to 0$. For small wavenumbers, the figure also displays ill-conditioning effects.

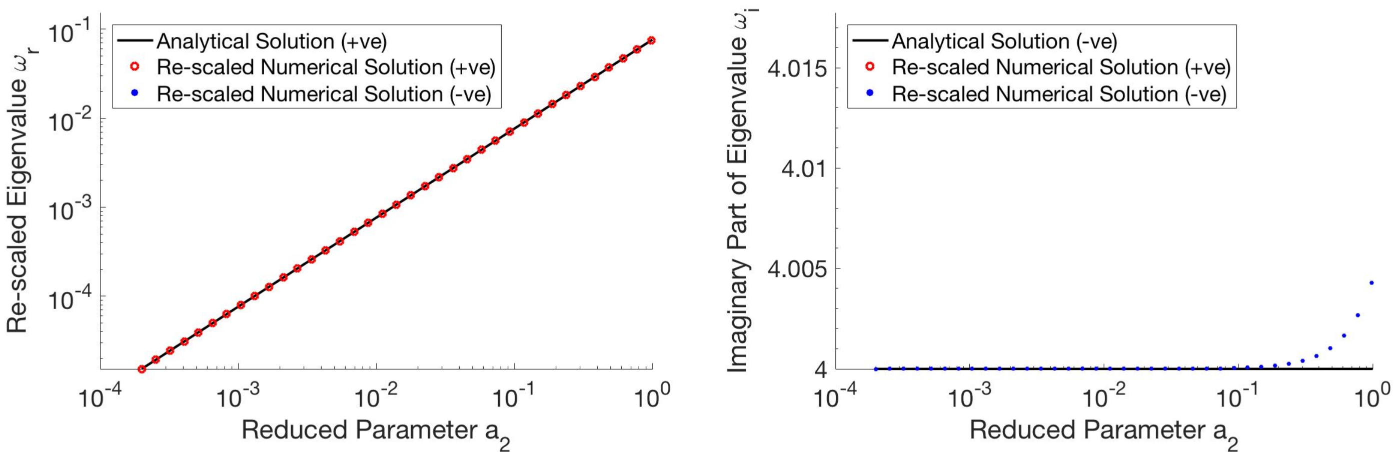

(a) Comparison for the real part, ω_r. (b) Comparison for the imaginary part, ω_i.

Figure S4: Analytical and re-scaled numerical solutions for the long wavelength advection regime.

3.5 Short Wavelength Acceleration

The analytical solution for the reduced model (6.23, 6.8 - 6.10) is given by,

$$\psi^{(0)} = \frac{2i\left(e^{-z^{(0)}(1-ia_1)} - e^{-z^{(0)}}\right)}{a_1}, \quad \omega^{(0)} = -2a_1 - 4i, \tag{S.27}$$

where $a_1 = F\mathrm{L}\mathrm{Re}\gamma\kappa\sin\theta$.

We compare the theoretical value of ω, given above, and the rescaled numerical results, $\omega_{\text{num}} = \frac{\omega}{F\mathrm{L}k^2\sin\theta}$ in Figure S5.

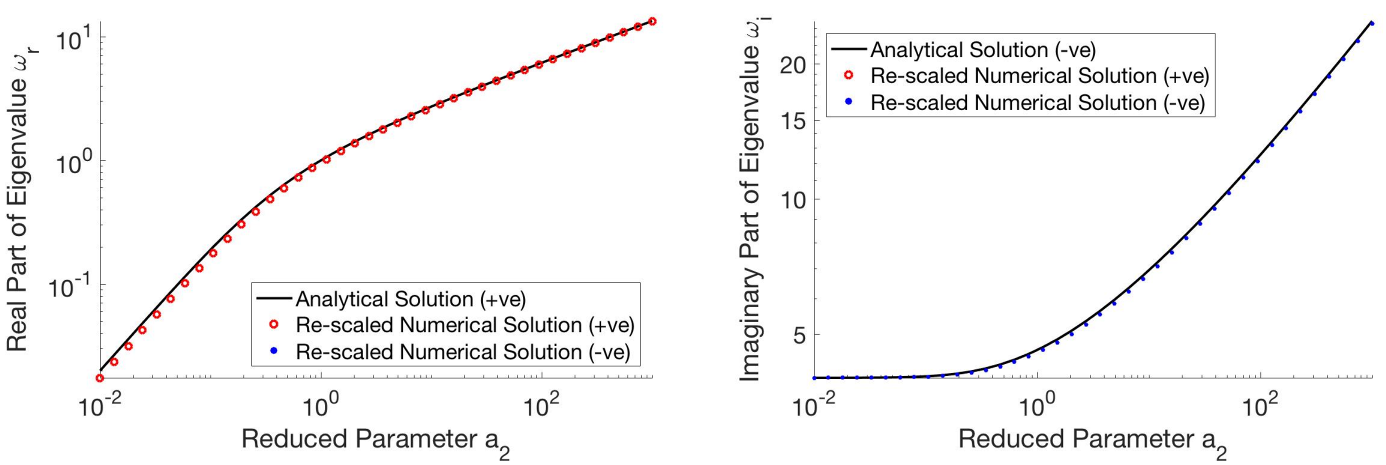

(a) Comparison for the real part, ω_r. (b) Comparison for the imaginary part, ω_i.

Figure S5: Analytical and re-scaled numerical solutions for the short wavelength advection regime.

3.6 Long Wavelength Acceleration

We reduce the re-scaled OS equation (6.13) for long wavelengths,

$$b_1\omega(D^{*2} - k^2)\psi^* = -ib_2\left[\left(2z^* - z^{*2}\right)(D^{*2} - k^2) + 2\right]\psi^* + (D^{*2} - 1)^2\psi^*, \tag{S.28}$$

by $b_1 \to 0$ to suppress acceleration, and an asymptotic expansion around $k = 0$ for the long wavelength regime,

$$b_1 \omega^{(0)} \mathrm{D}^2 \psi^{(0)} = \mathrm{D}^4 \psi^{(0)}. \tag{S.29}$$

This linear ordinary differential equation has characteristic roots, $0, 0, \pm\sqrt{b_1 \omega^{(0)}}$. We use the Matlab symbolic toolbox to solve the above equation. along with associated boundary conditions in the long wavelength regime (6.17 - 6.19), for $0 \le z \le 2$. We then symbolically compute $\mathrm{D}^2\psi^{(0)}$ as a function of $\sqrt{b_1\omega^{(0)}}$. Assuming $b_1 < 1$, which is justified since $\mathrm{L} \ll 1$, we perform a second-order Taylor expansion of $\mathrm{D}^2\psi^{(0)}(0)$ around $\sqrt{b_1\omega^{(0)}} = 0$ to get,

$$\mathrm{D}^2\psi^{(0)}(0) \approx A_0 + A_2 \left(\sqrt{b_1\omega^{(0)}}\right)^2, \quad A_0 = 3.7584, \quad A_2 = 2.2014. \tag{S.30}$$

The Exner equation yields,

$$\omega^{(0)} = \frac{A_0}{i - A_2 b_1}. \tag{S.31}$$

We compare the theoretical value of ω, given above, and the rescaled numerical results, $\omega_{\text{num}} = \frac{\omega}{F\mathrm{L}k\sin\theta}$ in Figure S6.

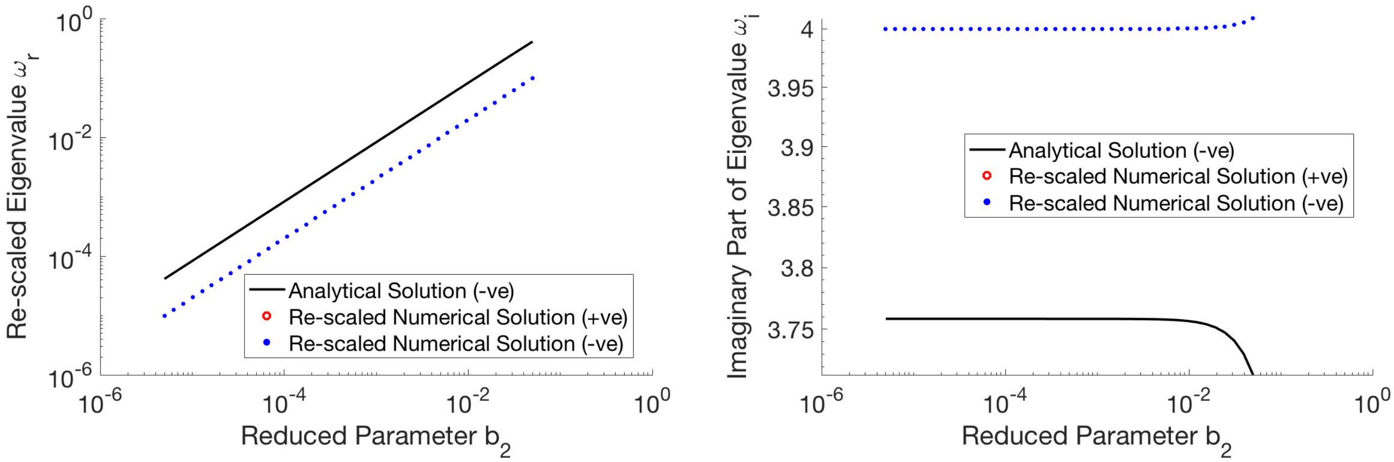

(a) Comparison for the real part, ω_r.

(b) Comparison for the imaginary part, ω_i.

Figure S6: Analytical and re-scaled numerical solutions for the long wavelength acceleration regime.